ELSEVIER

International Journal of Mass Spectrometry 216 (2002) 185–202

International Journal of Mass Spectrometry

www.elsevier.com/locate/ijms

Gas-phase activation of silane, disilane and germane by actinide ions; and collision induced dissociation of metal oxide ions in TOF-MS

John K. Gibson*

Chemical Sciences Division, Oak Ridge National Laboratory, P.O. Box 2008, Oak Ridge, TN 37831-6375, USA

Received 27 November 2001; accepted 14 February 2002

Abstract

Gas-phase reactions of selected actinide metal ions, An^+, with silane, disilane and germane under minimally hyperthermal conditions were studied using a reflectron time-of-flight mass spectrometer (RTOF-MS). Both U^+ and Np^+ reacted with silane while Pu^+ was comparatively inert. The primary reactions with silane yielded the silylenes, $AnSiH_2^+$; secondary reactions gave $AnSi_2H_4^+$ and $AnSi_2H_2^+$ (An = U, Np). With disilane, single- and double-dehydrogenation by An^+ produced $AnSi_2H_4^+$ and $AnSi_2H_2^+$ for An = U and Np, while Pu^+ and Am^+ were inert. Oxo-ligation rendered plutonium reactive towards silane: UO^+, NpO^+ and PuO^+ each dehydrogenated disilane to give $AnOSi_2H_4^+$. With germane, selected lanthanide ions, M^+=Ln^+, were studied along with M^+=An^+. Germylenes, $MGeH_2^+$, were formed for M = Th, U, Np, Pu, Ce and Tb, while Am^+ and Tm^+ were inert. Secondary products were MGe_2^+ (M = Th, U, Np, Ce and Tb), $ThGe_3^+$ and $ThGe_4^+$. The results are assessed in the context of the electronic structures and energetics of the actinide (and lanthanide) ions. For comparison and to confirm consistency with previous studies, a few reactions of CH_4 and C_2H_6 with actinide ions were examined. The nature of anomalous peaks at ion flight times corresponding to "tetrahydride" ions, "AnH_4," upon introduction of both reactive and inert gases into the reaction region was examined in detail. It was concluded that these aberrant peaks were due to high-energy collision induced dissociation of actinide oxide ions, AnO^+, in the first field-free region of the RTOF-MS. The identification of this dissociation phenomenon nullifies a previous report of actinide hydride ions produced by reactions of An^+ with ethylene oxide. (Int J Mass Spectrom 216 (2002) 185–202) © 2002 Elsevier Science B.V. All rights reserved.

Keywords: Actinides; Silane; Disilane; Germane; Collision induced dissociation

1. Introduction

Reactions of d-block transition metal ions with hydrocarbons have been studied extensively [1,2] to elucidate fundamental aspects of transition metal organometallic chemistry. Studies of gas-phase chemistry of lanthanide [3–11] and actinide [12–16] ions with hydrocarbons have illuminated the role of the electronic structures and energetics of the f-block elements in dehydrogenation and cracking reactions under conditions uncomplicated by highly perturbing secondary interactions typically encountered in condensed phase chemistry. Whereas small alkanes are generally relatively inert towards activation by gas-phase metal ions, the homologous silanes and germanes should be substantially more reactive due to a variety of factors, including weaker bonds and greater polarizabilities.

* E-mail: gibsonjk@ornl.gov.

1387-3806/02/$ – see front matter
PII S1387-3806(02)00584-5

The several studies of gas-phase reactions of transition metal ions with silane, SiH_4, confirm a substantially greater reactivity compared with methane [17–27]. Because reactions studied by the laser ablation with prompt reaction and detection (LAPRD) technique employed in the present study occur under only minimally hyperthermal conditions, only exothermic reactions are considered in the discussion here of previous studies with silane. Kang et al. [17] examined reactions with first row transition metals and found that Co^+ and Ni^+ dehydrogenate SiH_4; exothermic reactions did not occur for Ti^+, V^+, Cr^+ or Fe^+. They established the product structures by collision induced dissociation (CID) as corresponding to metal silylenes, and estimated the bond dissociation energies, BDE[M^+–SiH_2], as $\sim$280 kJ mol^{-1} for M = Co and Ni. The postulated mechanism was initiated by insertion of the metal ion into a Si–H bond to yield H–M^+–SiH_3. Irikura and Beauchamp [18] found that Os^+ exothermically reacted with silane to give $OsSiH_2{}^+$ and the silicides, $OsSi_{1,2,3}{}^+$. Both Sc^+ [20] and W^+ [26] induce dehydrogenation to silylenes and subsequent oligomerization to species including the dimers, $ScSi_2H_4{}^+$ and $WSi_2H_2{}^+$. Kickel and Armentrout [22–25] examined reactions of silane with all of the first row transition metal ions as well as Y^+, La^+ and Lu^+. The formation of $MSiH_2{}^+$ was found to be exothermic only for Ni^+, Cu^+, Y^+ and La^+. Reactions of gas phase metal ions with disilane, Si_2H_6, and germane, GeH_4, have been largely neglected.

Our particular interest in the field of gas-phase chemistry of actinide ions (An^+) is the role of the 5f electrons. It has been demonstrated that the 5f electrons of the actinide ions beyond Np^+ are chemically inert in hydrocarbon activation. The present study extends gas-phase actinide ion chemistry to reactions with silane, disilane and germane. Because of the greater susceptibility of these substrates to activation, it is of interest to compare the An^+–methane and An^+–ethane reaction systems with the corresponding silicon and germanium hydride substrates. Selected reactions with a few lanthanide ions (Ln^+) were studied for comparison. Also, the effects of oxo-ligation were assessed in the chemistry of some AnO^+ ions.

The studies with methane and ethane carried out in conjunction with the silane/germane studies revealed aberrant results, the origins of which were pursued. The implications of this anomalous behavior on the interpretation of previous experimental data for reactions of actinide ions with ethylene oxide is discussed.

2. Experimental

The experimental apparatus and procedures, LAPRD, have been described in detail elsewhere [10,16,28] and only a brief summary is provided here. The $\sim$10 ns duration, 308 nm wavelength pulse from a XeCl excimer laser was focused onto an ablation target to generate metal and metal oxide ions. The ablation targets were pellets of a copper matrix containing $\sim$1–5 atomic percent of each of two or more metal oxides. Under conditions where substantial amounts of actinide and lanthanide ions were ablated only minimal amounts of Cu^+ were produced, and the chemistry of the copper ions could not be meaningfully assessed. As discussed below, in those cases where the metal oxide ion bond dissociation energies were sufficiently large, substantial amounts of oxide ions were ablated along with the bare metal ions.

Ions were ablated into a reaction zone $\sim$3 cm long. The ion trajectory was approximately orthogonal to an adjacent pulsed valve which injected reagent gases in synchronization with the laser pulse. The nominal reagent pulse duration was $\sim$200 μs. All experiments were carried out using an acquisition rate of 5 spectra per second. With the pulsed valve operating at 5 Hz, a nearly constant reagent pressure in the range of 5×10^{-6} to 5×10^{-5} Torr was measured at an ionization gauge located near the ion mirror at the rear of the $\sim$1 m long reflectron time-of-flight mass spectrometer (RTOF-MS). The ambient background pressure was $\leq 1 \times 10^{-6}$ Torr, and for most experiments the measured quasi-static reagent pressure was $\sim 2 \times 10^{-5}$ Torr. The actual pressures in the reaction zone and the flight tube could not accurately be derived from the measurements at the ionization gauge. However, it is certain that the pressure in the reaction zone immediately

after ablation was much greater than the measured downstream pressure (i.e., $>10^{-4}$ Torr). Based on the observation of product ions resulting from sequential reactions with more than one reagent molecule, it can be assumed that a typical ablated ion encountered a reagent molecule; this suggests a transient local pressure in the reaction zone of *at least* 10^{-3} Torr. The pressure in the flight tube was presumably somewhat greater than the pressure measured near the ion mirror. No corrections were made for variable ionization gauge sensitivities for the different gases, due to the qualitative nature of the experiments.

Application of a +200 V pulse to a plate at the rear of the ion source injected both unreacted and product positively charged ions into the flight tube of the RTOF-MS (Comstock Model RTOF-210). The ions were accelerated to −2 kV upon entering the first field-free region of the RTOF-MS and were reflected in a gridless ion mirror with second order energy focusing. The mass spectrometer incorporates a channelplate detector at the rear of the ion mirror so that it is possible to obtain TOF mass spectra for unreflected ions by operating in the linear mode with diminished resolution and sensitivity.

The time delay between the laser pulse and injection of product ions into the RTOF-MS was typically ∼40 μs but was varied between 35 and 50 μs to optimize detected product ion yields. Under these conditions, the velocities of the sampled ions were $\sim 10^3$ m s^{-1} and the kinetic energy of an actinide ion with this velocity is ∼120 kJ mol^{-1}. The maximum center of mass collisional energies (KE_{CM}) for the actinide ion–molecule reactions were ∼10 kJ mol^{-1} for silane, ∼25 kJ mol^{-1} for disilane and ∼30 kJ mol^{-1} for germane. These are maximum KE_{CM} and all ions were studied under comparable conditions; however, the reaction conditions were certainly somewhat hyperthermal and some of the reported reactions may accordingly have been slightly endothermic.

All experiments were carried out in the Transuranium Research Laboratory at ORNL which is a facility specifically designed for handling “bulk” (i.e., non-tracer) quantities of transuranic actinides, several of which are produced in the nearby High Flux Isotope Reactor. The source region of the RTOF-MS is isolated inside of a sealed negative pressure air atmosphere glove box to prevent the release of radioactive contamination. The flight tube protrudes out of the rear of the glove box through an O-ring seal, and the vacuum pump, ion mirror, linear-mode detector and ion gauge are located outside of the glove box. All sample handling is performed in the glove box, and the laser beam enters the box through a quartz window in a side wall. The apparatus is contaminated with alpha emitting transuranic actinides to an extent that all maintenance must be performed in situ, substantially hampering the ability to repair or modify the instrument. Certain procedures, such as those which require removal of the flight tube, are entirely impractical. Because of the rather unusual design of the system, it is not feasible to accurately estimate local pressures under conditions of a constant reagent leak into the reaction zone; such estimates for pulsed valve operation, as in the work reported here, are even less reliable. The turbopump is located approximately mid-way down the flight tube, with several baffles between it and the reagent inlet, and the ion gauge is in a tube attached to the side of the vacuum chamber in which the flight tube is contained. Under typical pulsed valve operation at a repetition rate of 5 Hz, the ion gauge indicates only minor fluctuations in pressure. Spatial and temporal pressure variations of several orders of magnitude can be presumed between the pulsed valve and ion gauge. Reasonably quantifying the time-variable pressure gradient between the reaction zone and the tortuous route to the distant ion gauge is not practical, and accordingly only approximate estimated pressures are cited.

The reagent gases were all commercial products (Aldrich). The silane, disilane and germane each had a specified purity of at least 99.99%. The purities of the methane and ethane were both at least 99%.

Two potential complications of the LAPRD technique are the presence of a significant population of nascent excited state laser ablated metal ions, M^{+*}, in the reaction region; and the simultaneous presence of naked and oxo-ligated metal ions in the reaction region. That the LAPRD results reflect the chemistry of ground state (or nearly ground state) metal

ions, at least for the lanthanides and actinides, has been well-established by previous experiments and essentially remains a phenomenological observation [10,16,28]. That reaction pathways involving cleavage of a metal–oxygen bond can be excluded from consideration has also been experimentally demonstrated and reflects that only metal oxide ions with exceptionally strong bonds are ablated in significant quantities [10,16,28]; this issue is discussed in greater detail below.

3. Results and discussion

The results for reactions of the metal ions with small hydrocarbons are presented to establish the reliability of the LAPRD experimental approach by comparison with results obtained using other techniques. The hydrocarbon results also provide a basis for direct comparison with reactions of the silane and germane homologs. A series of experiments to account for anomalous results with the hydrocarbons was carried out with the conclusion that mass spectral peaks previously attributed to metal hydride ions were actually due to dissociation processes in the mass spectrometer. The results for reactions with silane, disilane and germane are presented and discussed in the context of the electronic structures of the metal ions, and compared with results reported in the literature for d-block transition metals. The main results are summarized in Tables 1 and 2, and Figs. 1–5. Ion intensities were measured as peak heights.

3.1. Reactions with methane and ethane

Reactions of actinide and lanthanide ions (and Zr^+) with the relatively inert alkanes, methane and ethane [1,2], were carried out to provide a basis for comparison with results for the silane and germane homologs. The appearance of peaks corresponding to flight times for products 3–4 amu above those of the bare metal ions is discussed in detail in the following section. Essentially, these anomalous peaks are not attributed to products of chemical reactions between the M^+ or $MO_{1,2}{}^+$ and the reagent ions, but rather to CID of MO^+ in the RTOF-MS.

Table 1
Product ion yields for reactions with silane and disilane[a]

	Product ion yield (%)		Product ion yield (%)
U–Pu + SiH_4			
$USiH_2{}^+$	2.3	$PuSiH_2{}^+$	<0.2
$USi_2H_4{}^+$	1.4	$PuSi_2H_4{}^+$	<0.08
$USi_2H_2{}^+$	0.8	$PuSi_2H_2{}^+$	<0.08
Np–Pu + SiH_4			
$NpSiH_2{}^+$	0.5	$PuSiH_2{}^+$	0.1
$NpSi_2H_4{}^+$	0.15	$PuSi_2H_4{}^+$	<0.04
$NpSi_2H_2{}^+$	0.06	$PuSi_2H_2{}^+$	<0.04
U–Pu + Si_2H_6			
$USi_2H_4{}^+$	5.1	$PuSi_2H_4{}^+$	<0.05
$USi_2H_2{}^+$	1.8	$PuSi_2H_2{}^+$	<0.05
$UOSi_2H_4{}^+$	0.6	$PuOSi_2H_4{}^+$	0.9
Np–Pu + Si_2H_6			
$NpSi_2H_4{}^+$	6.7	$PuSi_2H_4{}^+$	<0.03
$NpSi_2H_2{}^+$	0.9	$PuSi_2H_2{}^+$	<0.03
$NpOSi_2H_4{}^+$	1.1	$PuOSi_2H_4{}^+$	1.4
Np–Am + Si_2H_6			
$NpSi_2H_4{}^+$	2.0	$AmSi_2H_4{}^+$	<0.09
$NpSi_2H_2{}^+$	0.4	$AmSi_2H_2{}^+$	<0.09
$NpOSi_2H_4{}^+$	0.5	$AmOSi_2H_4{}^+$	ND[b]

[a] Product ion yields are given as a percent of the parent ion, M^+ or MO^+, ablated into vacuum. Upper limits are given for undetected products.

[b] ND: not detected; the amount of AmO^+ for reaction was too minuscule to report a significant upper limit.

Among the studied metal ions, only Th^+ was found to react with methane and ethane within the detection limits. Results for the reaction of Th^+ with methane are shown in Fig. 1; note that the peak there which apparently corresponds to "$ThH_4{}^+$" is actually attributed to Th^+ resulting from the CID process described below. With methane and ethane, the only significant reactions were the following three:

$$Th^+ + CH_4 \rightarrow ThCH_2{}^+ + H_2 \quad (1)$$

$$Th^+ + C_2H_6 \rightarrow ThC_2H_4{}^+ + H_2 \quad (2)$$

$$Th^+ + C_2H_6 \rightarrow ThC_2H_2{}^+ + 2H_2 \quad (3)$$

Reaction (1) was barely detectable—the small peak in Fig. 1 marked with an asterisk is due to the $ThCH_2{}^+$

Table 2
Product ion yields for reactions with germane[a]

	Product ion yield (%)		Product ion yield (%)
U–Pu + GeH_4			
$UGeH_2^+$	28	$PuGeH_2^+$	≤1[b]
UGe_2^+	5.4	$PuGe_2^+$	<0.1
UGe_3^+	<0.2[c]	$PuGe_3^+$	<0.1[c]
Np–Pu + GeH_4			
$NpGeH_2^+$	10	$PuGeH_2^+$	0.3
$NpGe_2^+$	2.7	$PuGe_2^+$	<0.1
Np–Am + GeH_4			
$NpGeH_2^+$	6	$AmGeH_2^+$	<0.2
$NpGe_2^+$	1.8	$AmGe_2^+$	<0.1
Th–Ce + GeH_4			
$ThGeH_2^+$	14	$CeGeH_2^+$	11
$ThGe_2^+$	4.4	$CeGe_2^+$	0.9
$ThGe_3^+$	0.6	$CeGe_3^+$	<0.1
$ThGe_4^+$	0.4	$CeGe_4^+$	<0.1
Tb–Tm + GeH_4			
$TbGeH_2^+$	5	$TmGeH_2^+$	<0.15
$TbGe_2^+$	1.6	$TmGe_2^+$	<0.05

[a]Product ion yields are given as a percent of the parent ion, M^+, ablated into vacuum. Upper limits are given for undetected products.

[b]Estimate due to interference from $UGeH_2^+$.

[c]MGe_3^+ and MGe_4^+ were detected only for M = Th; limits for M = U and Pu are included for comparison.

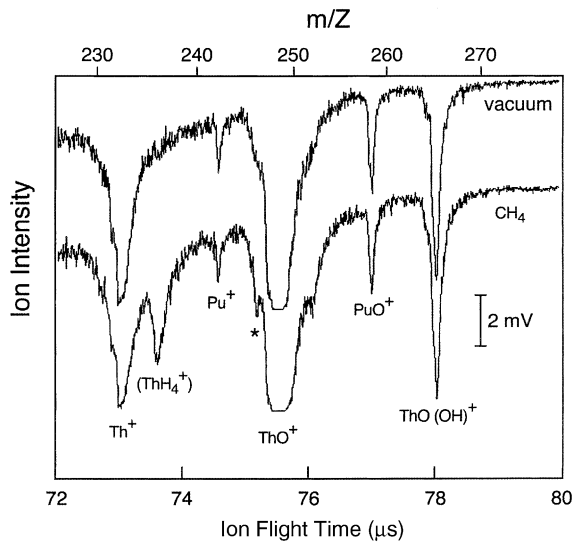

Fig. 1. Mass spectra for ablation of thorium ions into vacuum and methane. The asterisked (*) peak corresponds to the dehydrogenation reaction product, $ThCH_2^+$. The peak which appears at a flight time corresponding to "ThH_4^+" is considered to be due to Th^+ resulting from CID of ThO^+. The $^{242}Pu^+$ and $^{242}PuO^+$ peaks are due to plutonium contamination.

product. The overall reaction efficiency of Th^+ with ethane was substantially greater than with methane, as expected. With ethane, reaction (2) appeared to be somewhat more important than reaction (3). However, the $^{232}ThC_2H_2^+$ product of reaction (3) is isobaric with ablated $^{242}PuO^+$ ($^{242}PuO_2$ was a minor impurity in the target); this interference, similar to the PuO^+ peak evident in Fig. 1, precluded quantifying the relative importance of the reaction pathways (2) and (3). The results obtained here for Th^+ are consistent with those from a Fourier transform ion cyclotron resonance mass spectrometry (FTICR-MS) study by Marçalo et al. [14] which showed that reaction (1) is exothermic, albeit very inefficient, and that reaction channels (2) and (3) are of comparable importance.

No reaction products were observed with methane or ethane for any of the other metal ions studied, U^+, Np^+, Pu^+, Am^+, Ce^+, Ho^+, Tb^+, Tm^+ and Zr^+. The inert behavior of U^+ is consistent with FTICR-MS results [13]. A few FTICR-MS studies of reactions of lanthanide ions with small alkanes have been reported. In an early study, Schilling and Beauchamp [4] reported reaction cross-sections for Gd^+, one of the most reactive lanthanide ions, of 3×10^{-17} cm^2 with ethane and 4×10^{-14} cm^2 with 1-butene. Based on previous LAPRD results with for reactions of lanthanide ions with relatively reactive alkenes such as 1-butene, it was anticipated that reactions of Ln^+ with methane and ethane would not be detected in the present study. Similarly, the small rate constant for the reaction of Zr^+ with methane [29] and very low abundance of ablated Zr^+ is consistent with the absence of any detectable reaction products for Zr^+. The results for reactions with methane and ethane illustrate both the limited sensitivity of the LAPRD technique to metal ion reactions exhibiting low efficiencies, and consistency with FTICR-MS experiments regarding reaction channels

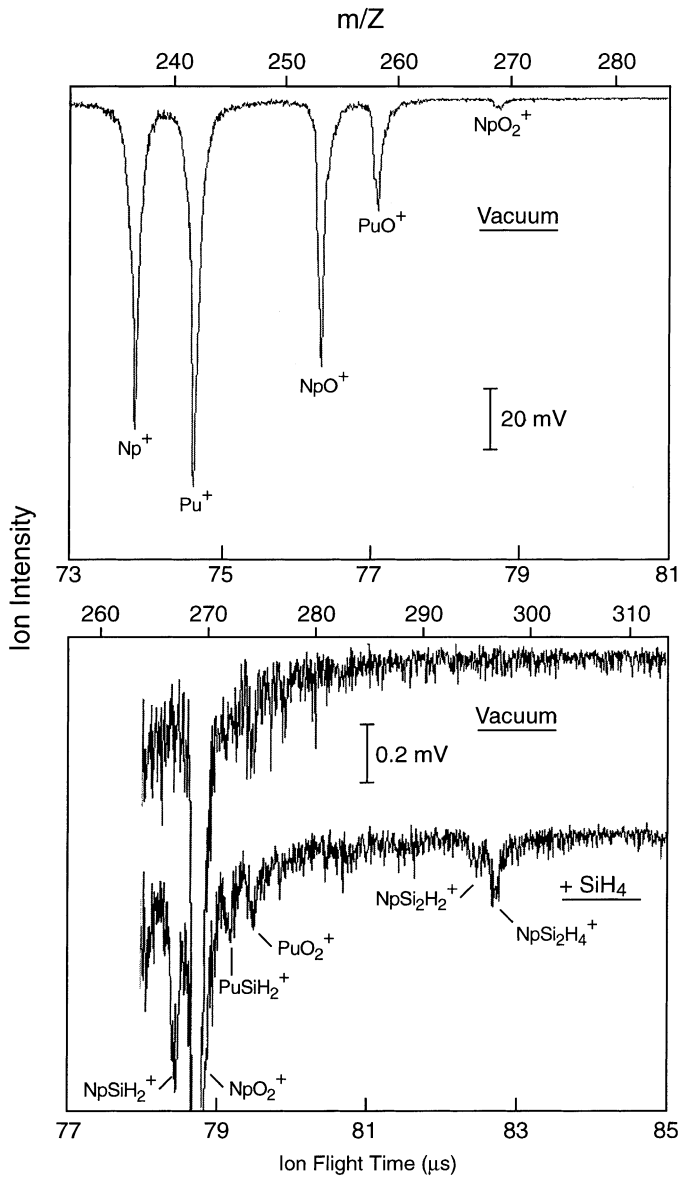

Fig. 2. Mass spectra for ablation of neptunium and plutonium ions into vacuum and silane. The top panel shows the low mass portion of the spectrum for ions ablated into vacuum. Ions due to reactions of ablated ions with silane are identified in the bottom spectrum in the lower panel.

and relative reactivities. As demonstrated previously for a wide variety of reactions, the LAPRD method reliably reveals ground state metal ion chemistry, and the main observed reactions correspond to exothermic processes.

3.2. CID of metal oxide ions

In the product mass spectrum shown in Fig. 1 the peak labeled ThH_4^+ suggests that Th^+ dehydrogenates methane. This initial interpretation of the

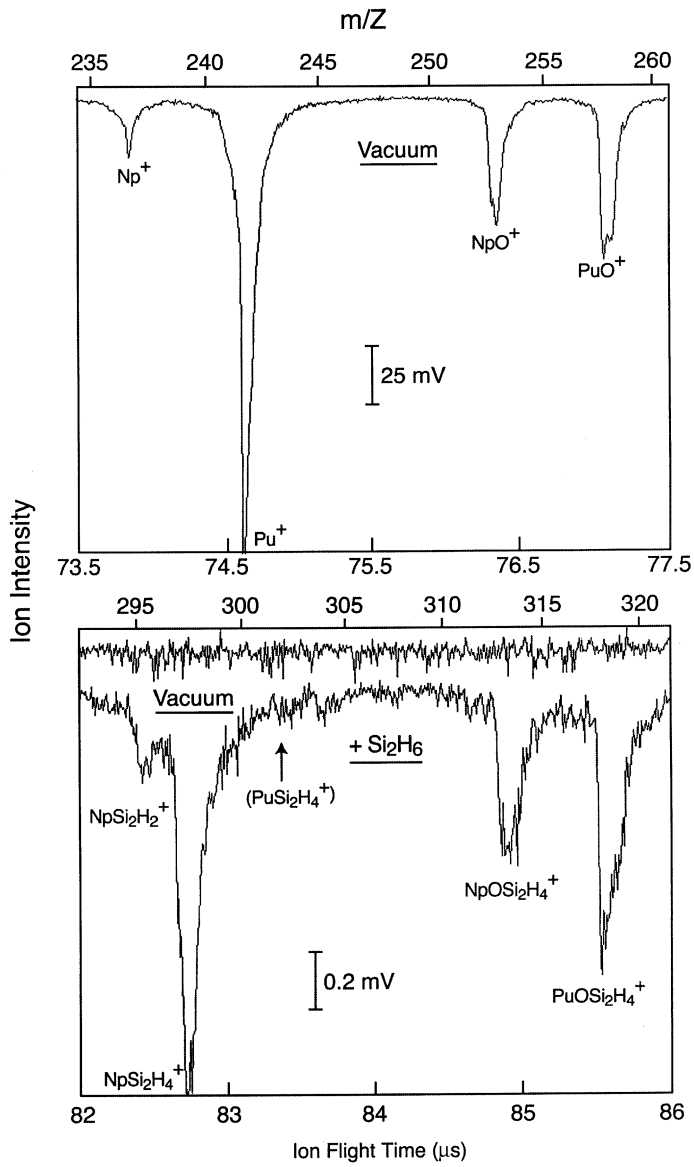

Fig. 3. Mass spectra for ablation of neptunium and plutonium ions into vacuum and disilane. The top panel shows the low mass portion of the spectrum for ions ablated into vacuum. Ions due to reactions of ablated ions with disilane are identified in the bottom spectrum in the lower panel.

mass spectrum would indeed suggest that ThH_4^+ is the primary product of the reaction of Th^+ with methane. However, an FTICR-MS study of this reaction [14] clearly demonstrated that the only significant channel was inefficient dehydrogenation to produce $ThCH_2^+$. Furthermore, it is highly implausible that a hydrogen-abstraction reaction could exothermically proceed: for example, BDE[U^+–H] is 276 kJ mol^{-1}, compared with a BDE[H_3C–H] of 439 kJ mol^{-1} [30].

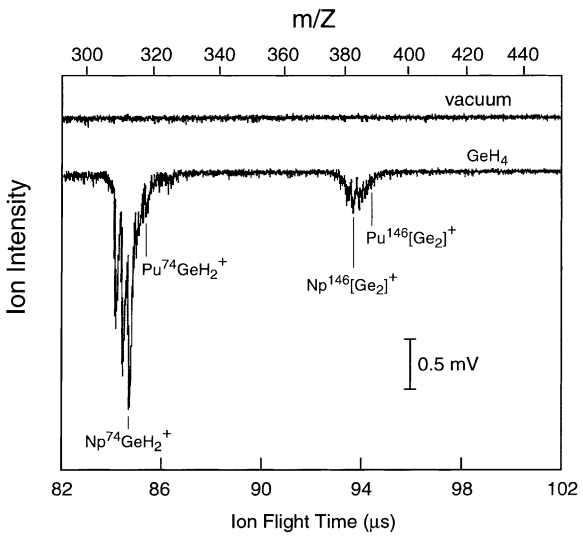

Fig. 4. Mass spectra for ablation of plutonium and neptunium ions into vacuum and germane with the primary reaction products identified. The amount of ablated Pu^+ was substantially greater than that of Np^+. Only a very minor amount of $PuGeH_2^+$ could be detected and $PuGe_2^+$ could not be definitively identified.

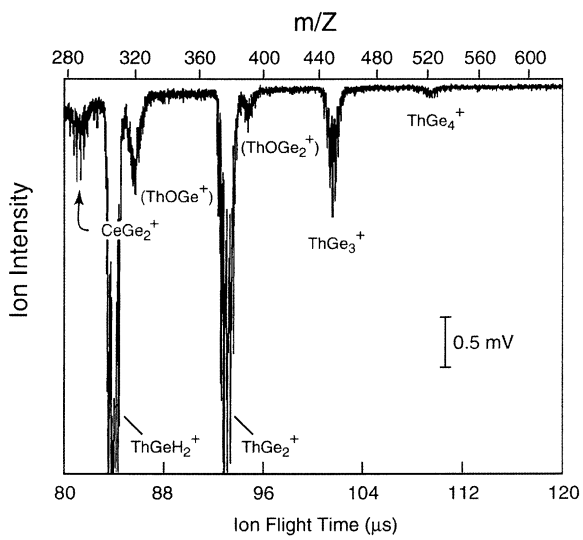

Fig. 5. Mass spectra for ablation of cerium and thorium ions into germane with the primary reaction products indicated. The yield of $CeGeH_2^+$ (not shown) was substantially greater than that of the minor $CeGe_2^+$ product (shown). The amount of ablated Th^+ was substantially greater than the amount of ablated Ce^+; the amounts of ablated ThO^+ and CeO^+ were comparable. The origins of the peaks tentatively identified as $ThOGe^+$ and $ThOGe_2^+$ are discussed in the text.

Similar peaks at flight times corresponding to ions with masses 3–4 amu greater than the ablated M^+ were observed for "reactions" with methane and/or ethane for the following metals: Th, U, Np, Pu, Ce, Tb and Zr. They were absent for Am, Ho and Tm, which also are the studied metals which produced primarily bare M^+, and only minuscule amounts of MO^+ upon ablation. The intensities of the abnormally broad anomalous peaks were typically between one and a few percent of the intensity of the ablated MO^+ peak. Further indication of a process related to ablated oxide ions was that the appearance of a "UOH_4^+" peak, an apparent "oxide hydride," was seen only for uranium—uranium was also unique in the ablation of substantial amounts of dioxide ion, UO_2^+. To confirm that these peaks which initially appeared to correspond to "hydride" products were not due to gas phase metal ion chemistry, ions were ablated into He and Ar injected into the reaction zone under the same conditions as reactive reagent gases. Peaks at flight times corresponding to species such as "NpH_4^+" and "PuH_4^+" also appeared with the inert gases. To exclude the possibility of reaction of metal ions with water contamination from the pulsed valve, the inlet system was saturated with D_2O. No additional peaks which could be attributed to deuterides appeared under these conditions, excluding the possibility of reactions with water. An experiment with ethylene oxide (EtO) was repeated to confirm the role of the dioxide parent ion. Whereas only "PuH_4^+" appeared with other pulsed gases, "$PuOH_4^+$" appeared with EtO. Only minuscule amounts of PuO_2^+ are directly ablated but EtO oxidizes PuO^+ to PuO_2^+. Although "$PuOH_4^+$" was absent for all other reagents, its yield was 1.5% that of the PuO_2^+ generated by oxidation with EtO. This yield is comparable to the yields of other "MH_4^+" and "MOH_4^+" relative to the amounts of directly ablated MO^+ and MO_2^+.

Evidently the "tetrahydride" peaks were not in fact reaction products but rather derived from parent oxide ions. It is proposed that CID of oxide ions in the first field-free region of the RTOF-MS results in fragment ions which appear at arrival times in close correspondence to the masses of hypothetical AnH_4^+. Metastable decay of a molecular ion in the

first field-free region of an idealized single stage RTOF-MS results in an arrival time for the daughter ion, t_d, which is related to the arrival time of the parent ion, t_p, by the following relationship, where m_d is the mass of the daughter ion and m_p that of the parent ion [31]:

$$t_d = \left[\frac{t_p}{2}\right]\left[\frac{m_d}{m_p} + 1\right] \quad (4)$$

It is predicted that daughter fragment ions will arrive at the reflected ion detector before parent ions. The gridless ion mirror with second order energy focusing reflectron used in the present work can be treated approximately as a dual-stage reflectron [31]. As discussed by Cotter [31], metastable decay in single and dual-stage reflectrons can be treated similarly when $(m_d/m_p) \geq 0.8$. To assess the relevance of Eq. (4) to the present results, measurements were made for $^{90}Zr^+/^{90}ZrO^+$, $^{142}Ce^+/^{142}CeO^+$ and $^{232}Th^+/^{232}ThO^+$ all simultaneously ablated into methane. Peaks were observed which corresponded to $Zr[3.0]^+$, $Ce[3.4]^+$ and $Th[3.8]^+$, where the numbers in brackets represent the calculated mass above the parent ion based on the assumption of injection of stable ions from the ion source into the mass spectrometer. The measured t_d for these three anomalous peaks are well-represented by Eq. (5), where the CID parent ion is assumed to be MO^+ and the daughter M^+.

$$t_d = \left[\frac{t_p}{1.98}\right]\left[\frac{m_d}{m_p} + 1\right] \quad (5)$$

It is not surprising that the CID of oxide ions in our RTOF-MS cannot be treated exactly as metastable decay in an idealized single stage reflectron according to Eq. (4). However, approximate applicability of Eq. (4) is expected because the m_d/m_p were in the range of 0.85 for ZrO^+ to 0.94 for ThO^+. The similarity between Eqs. (4) and (5) is clearly consistent with MO^+ dissociation in the first field-free region.

Terbium and thulium oxides were ablated into EtO while a variable voltage applied to the ion mirror was altered from the standard optimal value of −1.044 to −1.102 kV. As discussed by Gilmore and Seah [32], altering the ion mirror voltage parameters should generally have different effects on ions which remain intact throughout their trajectory in the RTOF-MS compared with ions which undergo decay in the first field-free region. With the more negative variable voltage, net flight times decreased for all ions and a new mass calibration constant was derived from the flight time of ablated Tb^+. The mass of ablated $^{169}Tm^+$ calculated from this new calibration constant was exactly 169 amu, as expected for a stable bare metal ion injected into the flight tube. However, the *apparent* masses of the two anomalous peaks were distinctly shifted up, from $M[3.7]^+$ (for −1.044 kV) to $M[4.3]^+$ (for −1.102 kV), for both M = Tb and Tm. These shifts in *apparent* masses provide further evidence that these latter peaks do not correspond to stable ions injected from the ion source.

Confirmation that the anomalous peaks were due to dissociation in the first field-free region of the RTOF-MS was obtained by obtaining reflectron and linear TOF mass spectra under essentially identical source conditions. If the anomalous ("hydride") peaks were due to the postulated CID process in the field-free region, they would not appear using the linear mode. The mass spectrometer was operated in a modified configuration which allowed obtaining mass spectra for unreflected ions using a channelplate detector at the back of the ion mirror. The resolution and sensitivity of the linear mode mass spectra was reduced, but adequate to ascertain the nature of the anomalous peaks. Again, Tb and Tm ions were studied using EtO as the reactant gas. In both the reflectron and linear modes, peaks due to the primary oxidation products such as TmO^+ were clearly evident at the predicted flight times. In the reflectron mode, a peak corresponding to $Tb[3.6]^+$ was evident with an intensity comparable to that of the Tm^+ peak. In the linear mode this peak was absent to the detection limit of ≤1% relative to the Tm^+ peak. This result is consistent with a dissociation process in the first field-free region as the origin of the broad peaks at slightly longer flight times than the bare M^+ upon operation in the reflectron mode.

It is not possible to accurately predict the probability of CID of metal oxide ions under the LAPRD

experimental conditions due to uncertain pressures in the flight tube, and uncertain oxide ion dissociation cross sections. However, the validity of the proposed degree of CID can be qualitatively assessed. The ion flight path in the first field-free region is ∼100 cm. For 2 keV $AnO_{1,2}^+$ ions, the center-of-mass collisional energies (KE_{CM}) ranged from ∼30 eV with He as the target gas to ∼300 eV with EtO as the target. Armentrout and Beauchamp [33] studied the CID of UO^+ and UO_2^+ using Ar as the collision gas. They found a maximum dissociation cross-section, σ, for UO^+ of 4×10^{-17} cm^2 for $KE_{CM} \approx 20$ eV and a maximum s for UO_2^+ of 9×10^{-17} cm^2 for $KE_{CM} \approx 15$ eV. The apparent dramatic decrease in both cross sections to $<10^{-17}$ cm^2 above $KE_{CM} = 30$ eV may have been due to increased ion scattering at high collisional energies. Results from Sievers et al. [34] suggest maximum CID cross-sections for YO^+, ZrO^+, NbO^+ and MoO^+ colliding with Xe of the order of $\sim 10^{-16}$ cm^2 at KE_{CM} around 30 eV. A *maximum* CID cross-section of $\sim 10^{-16}$ cm^2 is estimated for the actinide and lanthanide oxide ions. Finally, a neutral species number density in the flight tube of the order of 10^{12} cm^{-3} ($\sim 3 \times 10^{-5}$ Torr) is estimated based on the quasi-static pressure measured at the ion gauge while the pulsed valve was operating at 5 Hz. As noted above, this pressure is only a rough estimate to allow a qualitative assessment of the expected extent of collisional dissociation. The resulting predicted probability for CID of a metal oxide ion in the first field-free region prior to entering the ion mirror is of the order of 0.01 (∼1%), in reasonable agreement with the magnitudes of the anomalous peaks relative to those of the oxide ions which are postulated as precursors.

The comparable phenomenon of decomposition of high energy organic ions after excitation has been a topic of study for more than three decades (early and recent examples are found in [35–39]). In the present study, introduction of an inert or reactive gas substantially decreased the intensities of the detected ablated ions, presumably due to scattering in the flight tube. The diminution of the metal oxide ion signal upon introducing a reagent or inert gas was much greater than the CID peak intensity, indicating that the probability of scattering of a metal oxide ion was much greater than the probability of dissociation under our experimental conditions. For comparison, McLafferty et al. [40] found that ion scattering became dominant over dissociation when a certain number of ion–neutral collisions was exceeded. This occurred above pressures of $\sim 10^{-4}$ Torr for 3.75 keV nitrobenzene ions in an ∼50 cm long collision region containing Ar [40]. The cross-sections for high-energy CID of large molecular ions would be expected to be greater than those for small diatomic ions such as MO^+. Spengler et al. [41] measured cross sections of greater than 10^{-13} cm^2 for CID of 20 keV cytochrome *c* ions colliding with nitrogen. The high-energy dissociation of MO^+ might be comparable to the excitation of small molecular ions according to the *electronic mechanism* described by Fayeton et al. [42] in their study of the CID of Na_2^+. In this mechanism, the fragments are forward-scattered, in accord with the appearance of a discrete, albeit broadened, fragment ion peak, M^+, in the RTOF-MS metal oxide ion CID spectra.

It is concluded that the previous assignments of "AnH_4^+" and "$AnOH_4^+$" as minor products of reactions of ethylene oxide with An^+ and AnO^+ [43] were incorrect and that no such "tetrahydrides" were actually produced. Furthermore, similar peaks with intensities in accord with CID of AnO^+ appeared in reactions with silanes and germane but are not considered in the following presentation and discussion of those results. For example, a peak at a flight time corresponding to a mass 3.5 amu greater than that of Pr^+ which appeared upon reaction with disilane is presumed due to CID of PrO^+ and is not considered a reaction product. It should be noted that the oxide CID phenomenon does not alter the interpretation of the primary results of the LAPRD studies; only the attribution of oxide ion CID peaks as "hydride" products is considered incorrect. Most earlier LAPRD experiments were carried out at lower pressures in the RTOF-MS flight tube so that the probability of CID was greatly diminished. However, close re-examination of some previous results reveals very small peaks which probably did result from metal oxide ion CID; these features were too minor to consider

as significant product ions except in the case of the high-pressure EtO experiments. In the present series of experiments with germane at relatively high pressures, another possible manifestation of molecular ion CID was identified, as discussed below.

3.3. Reactions with silane

Representative results for reactions with silane are shown in Fig. 2. The major ion–molecule reaction products and their yields as a percentage of the amount of parent ion ablated into vacuum, prior to injection of the reactant gas, are given in Table 1. Because products attributed to reactions of MO^+ with disilane are included in Table 1, it should be noted that no products of any reactions of MO^+ with silane or germane nor any reactions whatsoever of $UO_2{}^+$, the only dioxide ion ablated in appreciable amounts, were detected to a sensitivity of ∼0.1%. It should also be noted that the range of experiments carried out to study reactions with silanes and germane were restricted by the particular hazards involved in handling pyrophoric gases in conjunction with radioactive transuranium materials. During the studies with silane, spontaneous ignition occurred within the sealed vacuum exhaust system of the transuranium handling facilities.

The U–Pu and Np–Pu targets were ablated into silane. The ions ablated in sufficient quantity for appreciable reaction in these two experiments were U^+, UO^+, $UO_2{}^+$, Pu^+ and PuO^+ for "U–Pu;" and Np^+, NpO^+, Pu^+ and PuO^+ for "Np–Pu." As noted above and discussed in detail elsewhere [16], the M^+–O and OU^+–O bonds of the ablated oxide ions were sufficiently strong—$BDE[M^+–O] \geq 700\,kJ\,mol^{-1}$—to exclude reaction pathways requiring cleavage of the M^+–O bonds. For example, the observed $USiH_2{}^+$ product ion could theoretically be attributed to either H_2-elimination from SiH_4 by bare U^+ or H_2O-elimination by UO^+. However, exothermic formation of a U^+–silylene complex from UO^+ reacting with silane by dehydration would require that $BDE[U^+–SiH_2]$ be at least $\sim 550\,kJ\,mol^{-1}$ (using $BDE[U^+–O] \approx 807\,kJ\,mol^{-1}$ [30]). In contrast, dehydrogenation of silane by U^+ is exothermic if $BDE[U^+–SiH_2]$ exceeds $\sim 230\,kJ\,mol^{-1}$. Because of the large $BDE[M^+–O]$ for all ions produced in significant amounts under the high-energy ablation conditions of LAPRD, exothermic dehydration by metal oxide ions can confidently be excluded based on thermodynamic considerations. Dehydrogenation by bare M^+ is confidently assigned as the reaction pathway for this and other reactions, and the MR^+ products can be attributed to reactions of M^+, not MO^+ or $MO_2{}^+$. In contrast, the reactivity of oxide ions such as FeO^+ [27] reflects the relatively weak Fe^+–O bond—$BDE[Fe^+–O] \approx 410\,kJ\,mol^{-1}$ [30]—and the resulting enhanced susceptibility to metal–oxygen bond cleavage.

As seen from the results in Table 1, U^+, Np^+ and Pu^+ each dehydrogenated silane to produce $MSiH_2{}^+$ according to reaction (6):

$$M^+ + SiH_4 \rightarrow MSiH_2{}^+ + H_2 \quad (6)$$

The thermochemical values in Table 3 indicate that dehydrogenation of silane to give the silylene ligand in products with a presumed M^+–SiH_2 structure [17] requires only $230\,kJ\,mol^{-1}$, in contrast to the $457\,kJ\,mol^{-1}$ needed to produce methylene from methane. The most striking result was that the reaction efficiencies of U^+ and Np^+ were both substantially greater than that of Pu^+. Although the two ions were not directly compared, it appears that the reactivity of U^+ may have been somewhat greater than that of Np^+. The appearance of a small amount of $PuSiH_2{}^+$ (Fig. 2) suggests that dehydrogenation of silane is an exothermic process for all three of these actinide ions and that the differences in reactivity can be attributed to a much lower reaction cross section for Pu^+. Assuming that activation of silane by an M^+ proceeds by an initial insertion, as postulated by others and in analogy with hydrocarbon activation [13,28], the initial H–M^+–SiH_3 intermediate requires the availability of two chemically active valence electrons at the metal center. If the quasi-valence 5f electrons of Pu^+ were effective at forming covalent bonds in such an intermediate, then the reactivity of Pu^+ should have been comparable to those of U^+ and Np^+. Instead, it appears that excitation of Pu^+ from the ground state

Table 3
Neutral reaction enthalpies at 0 K[a]

Precursor(s)	Products	$\Delta_f H$ (kJ mol^{-1})
CH_4	$CH_3 + H$	432
	$CH_2 + H_2$	457
	$C + 2H_2$	778
	$(1/2)C_2 + 2H_2$	479
SiH_4	$SiH_3 + H$	378
	$SiH_2 + H_2$	230
	$Si + 2H_2$	402
	$(1/2)Si_2 + 2H_2$	249
GeH_4	$GeH_3 + H$	344
	$GeH_2 + H_2$	158
	$Ge + 2H_2$	273
	$(1/2)Ge_2 + 2H_2$	135
C_2H_6	$C_2H_5 + H$	414
	$C_2H_4 + H_2$	129
	$C_2H_2 + 2H_2$	297
Si_2H_6	$Si_2H_5 + H$	368
	$Si_2H_4 + H_2$	188
	$Si_2H_2 + 2H_2$	289
$SiH_2 + SiH_4$	$Si_2H_4 + H_2$	−35
	$Si_2H_2 + 2H_2$	65

[a]Formation enthalpies (0 K) used to derive the net reaction enthalpies are from [30], except for the following: the $\Delta_f H[SiH_n]$ are from [22]; the $\Delta_f H[GeH_4]$ are from [44]; and the $\Delta_f H[Si_2H_n]$ are from [45]. The uncertainties range from a few kJ mol^{-1} (for some hydrocarbon reactions) up to ∼25 kJ mol^{-1} (for some reactions involving GeH_n or Si_2H_n). Because only qualitative comparisons are made, specific estimated uncertainties are not given.

to a reactive "divalent" configuration with two non-5f valence electrons is necessary for the reaction to proceed. As seen in Table 4, this promotion energy is 105 kJ mol^{-1}. The high reactivities of U^+ and Np^+ are attributed to the availability of two spin-unpaired valence electrons in the ground state (Np^+) or a very low-lying excited state (U^+). A detailed discussion of the requirements for metal ion bond activation has been provided by Armentrout [48].

The actinide results are consistent with those for reactions of La^+ and Lu^+ with silane reported by Kickel and Armentrout [24]. Dehydrogenation was found to proceed at very low collision energies for La^+ but required a KE_{CM} of ∼140 kJ mol^{-1} for Lu^+. The ground state of La^+ is [Xe]6d^2. In contrast, Lu^+ has a ground state configuration of [Xe]5f^{14}6s^2 with the [Xe]4f^{14}5d6s configuration 141 kJ mol^{-1} higher in energy [47]. The lanthanide ion results indicate that the closed shell 6s^2 configuration of Lu^+ cannot activate SiH_4 and that promotion to the 5d6s configuration is necessary, consistent with a H–Ln^+–SiH_3 activated intermediate. Kickel and Armentrout [24] discuss the relatively facile formation of group III (including lanthanide) silylenes, $MSiH_2^+$, compared with methylenes, MCH_2^+, based on both kinetic and thermodynamic considerations. From a kinetic perspective, the H–SiH_3 bond is ∼54 kJ mol^{-1} weaker

Table 4
Promotion energies for actinide and lanthanide ions, M^+[a]

M^+	Ground state configuration[b]		Lowest "divalent" configuration[b]		ΔE (kJ mol^{-1})
Th^+	$^4F_{3/2}$	6d^{2}7s	Ground	Ground	0
U^+	$^4I_{9/2}$	5f^{3}7s^2	$^6L_{11/2}$	5f^{3}6d7s	3
Np^+	$^7L_5$	5f^{4}6d7s	Ground	Ground	0
Pu^+	$^8F_{1/2}$	5f^{6}7s	$^8K_{7/2}$	5f^{5}6d7s	105
Am^+	$^9S_4$	5f^{7}7s	($^9H_1$)	5f^{6}6d7s	246
Ce^+	$^4H_{7/2}$	4f5d^2	($^2G_{9/2}$)	4f5d6s[c]	28[c]
Tb^+	$^7H_8$	4f^{9}6s	$^9G_7$	4f^{8}5d6s	39
Tm^+	$^3F_4$	4f^{13}6s	($^5K_5$)	4f^{12}5d6s	199

[a]The lowest "divalent" configuration is the lowest energy configuration with two non-f valence electrons. The lowest-lying level is used for a given configuration. The actinide ions energies are from [46]. The lanthanide ion energies are from [47].

[b]The electronic configurations exclude the inert core, Rn for the An^+ and Xe for the Ln^+.

[c]For Ce^+, there are two non-4f valence electrons in the ground state configuration, 4f5d^2. The energy for promotion to a state with one valence 5d-electron and one valence 6s-electron is given because all other M^+ have a ground or lowest-lying "divalent" configuration with one valence s-electron.

than the H–CH_3 bond (Table 3) and silane activation should be more facile than methane activation. Thermodynamically, dehydrogenation of methane requires 457 kJ mol^{-1} whereas dehydrogenation of silane requires only 230 kJ mol^{-1} (Table 3). In the case of lanthanum, for example, BDE[La^+–CH_2] is less than 170 kJ mol^{-1} larger than BDE[La^+–SiH_2] [2]. Accordingly, La^+-induced dehydrogenation of silane is thermodynamically more favorable than dehydrogenation of methane by ∼60 kJ mol^{-1}.

No metal silicides, MSi^+, were detected. As seen from the enthalpies in Table 3, complete dehydrogenation of SiH_4 requires 402 kJ mol^{-1}. The dissociation energy of neutral ScSi has been determined as 224 kJ mol^{-1} [49] and it can be predicted that BDE[An^+–Si] will be less than ∼402 kJ mol^{-1} required for exothermic complete dehydrogenation of silane by An^+.

The secondary silane reaction products reported in Table 1 correspond to dimerization of silane, probably according to reactions (7) and (8), where M = U and Np, indicating multiple ion–molecule collisions under the LAPRD experimental conditions.

$$MSiH_2^+ + SiH_4 \rightarrow MSi_2H_4^+ + H_2 \quad (7)$$

$$MSi_2H_4^+ \rightarrow MSi_2H_2^+ + H_2 \quad (8)$$

The yields of $MSi_2H_4^+$ and $MSi_2H_2^+$ ranged from ∼10 to ∼60% relative to the amount of remaining $MSiH_2^+$ reactant ion (M = U and Np). Although it is feasible that the $MSi_2H_2^+$ were produced by simultaneous loss of two H_2 molecules, an MSi_2H_4 intermediate (reaction (8)) is considered more probable. Considering only the thermodynamics associated with the reactions of the free silane species and not the indeterminate degree of bonding between the metal ion and the silicon hydride product ligands, the enthalpy for reaction (7) is approximately −35 kJ mol^{-1} and that for reaction (8) is ∼100 kJ mol^{-1} (Table 3). Both reactions (7) and (8) are almost certainly exothermic when the additional contribution from the bonding between the M^+ center and the $Si_2H_{2,4}$ ligands is included. Ruscic and Berkowitz [45] have predicted the structures of Si_2H_n species. Whereas the structure of Si_2H_4 is evidently ethene-like, $H_2Si{=}SiH_2$, that of Si_2H_2 is not comparable to that of ethyne but is instead cyclic with two bridging hydrogen atoms: Si–μ-{H/H}–μ-Si. These free molecule structures may be perturbed appreciably upon coordination to a metal ion.

Gas-phase oligomerization of silane has been reported for other metal ions. The reaction of Sc^+ with SiH_4 results in $ScSiH_2^+$ as the primary product; secondary products include $ScSi_2H_4^+$ and $ScSi_2H_2^+$ [20]. Ferhati et al. [26] studied the reaction of W^+ with silane and products included $WSiH_2^+$, $WSi_2H_2^+$, and larger oligomers up to $WSi_{10}H_6^+$. Notably, they did not observe the presumed $WSi_2H_4^+$ intermediate between the $\{WSiH_2^+ + SiH_4\}$ reactants and the $WSi_2H_2^+$ product. Experimental and theoretical assessments of the structure of $WSiH_2^+$ again indicated a metal silylene, formally $W^+{=}SiH_2$. The non-observance of $WSi_2H_4^+$ was attributed to rapid elimination of the second H_2 molecule to give $WSi_2H_2^+$. It was concluded that the structure of $WSi_2H_4^+$ is either a tungsten disilene comprising a WSi_2 ring, or a tungsten silylsilylene, $W^+{=}SiH(SiH_3)$. Three structures for $WSi_2H_2^+$ were estimated to be of comparable stability. Interestingly, none of the three incorporate the cyclic structure for isolated Si_2H_2 proposed by Ruscic and Berkowitz [45]. Reaction of Os^+ with SiH_4 [18] results in complete dehydrogenation under near thermal conditions to produce $OsSi^+$, $OsSi_2^+$ and $OsSi_3^+$. Whereas the $UO_{1,2}^+$, NpO^+ and PuO^+ were evidently inert towards SiH_4, it was found that OsO^+ dehydrogenated silane to produce $OsOSi^+$, $OsOSi_2^+$ and $OsOSi_3^+$ [18]. As with alkanes, osmium ions exhibit a very high reactivity with silane.

3.4. Reactions with disilane

Representative results for reactions with disilane are shown in Fig. 3 and the studied reactions and products are included in Table 1. Whereas all of the studied An^+ except Th^+ were inert towards ethane, both U^+ and Np^+ rather efficiently dehydrogenated and double-dehydrogenated disilane to produce $MSi_2H_4^+$ and a smaller amount of $MSi_2H_2^+$. In contrast, both

Pu^+ and Am^+ were essentially inert. The primary dehydrogenation product ion implies reaction (9), where M = U and Np.

$$M^+ + Si_2H_6 \rightarrow MSi_2H_4^+ + H_2 \quad (9)$$

Considering the promotion energies in Table 4, the occurrence of reaction (9) for U^+ and Np^+ but not Pu^+ and Am^+ indicates dehydrogenation via an insertion intermediate, H–An^+–SiH_2–SiH_3, with the requirement for two non-5f electrons at the metal center to form the two covalent bonds. As with hydrocarbons, the 5f electrons of Pu^+ and $Am^+$are evidently unable to effectively participate in covalent bonding upon interacting with disilane. It is assumed that the second H_2-loss occurs via an $AnSi_2H_4^+$ intermediate, according to reaction (8). However, it is not evident whether the second dehydrogenation proceeds by a direct An^+ insertion, which would require a non-covalently bonded metal center in the $AnSi_2H_4^+$ complex so that the An^+ metal center would be available for a second insertion into a Si–H bond.

In view of thermodynamic considerations [22,30], it is notable that Si–Si activation to produce metal silylenes and silane is not a significant reaction pathway. The formation of SiH_2 and SiH_4 from disilane requires only 225 kJ mol^{-1}. This contrasts with the 391 kJ mol^{-1} required to produce methylene and methane from ethane. Accordingly, the metal–silicon bond energy in M^+–SiH_2 would have to be only >225 kJ mol^{-1} for silylene formation to be exothermic. The observed production of $MSiH_2^+$ from reactions of M^+ (M = U, Np and Pu) with silane indicates that BDE[M^+–SiH_2] $\geq$ 230 kJ mol^{-1}. However, the Si–Si bond energy in disilane is 316 kJ mol^{-1}, compared with the C–C bond energy of 366 kJ mol^{-1} in ethane. For both ethane and disilane, H_3X–XH_3, X–H activation is evidently favored over X–X activation (X = C and Si), with these metal ions.

An additional product from reaction with disilane not included in Table 1 was $USi_4H_4^+$, at only ~0.2% yield relative to U^+ ablated into vacuum. The precursor to this is probably $USi_2H_2^+$, suggesting that the net reaction (10) proceeds, through an unknown mechanism.

$$USi_2H_2^+ + Si_2H_6 \rightarrow USi_4H_4^+ + 2H_2 \quad (10)$$

In the reaction of W^+ with SiH_4 [26] $WSi_4H_4^+$ was identified as one of the several oligomerization products. Although it is not possible to definitively assign a structure to $USi_4H_4^+$ (or $WSi_4H_4^+$), a reasonable possibility is a U^+ coordinated to a ring comprised of four Si–Si bonded silylidyne units, U^+-η^4-cyclo-$(SiH)_4$.

The relative reactivities of the bare An^+ towards disilane confirm that Si–H activation proceeds via an insertion mechanism which requires two non-5f electrons at the metal center, in direct analogy with C–H activation. In distinct contrast to the large differences apparent in the reactivities of the bare metal ions, the three AnO^+ ablated in adequate amounts to detect reactions each dehydrogenated disilane to produce $MOSi_2H_4^+$ (M = U, Np and Pu) with comparable efficiencies. Whereas Pu^+ was nearly inert compared with U^+ and Np^+, PuO^+ was apparently slightly more efficient at dehydrogenating disilane than were UO^+ and NpO^+.

In studies of activation of butadiene by LnO^+, Cornehl et al. [50] postulated electrophilic attack on the π-system by the oxide ion. In a comparative study of the gas-phase chemistry of NdO^+ and its actinide homolog, UO^+, Cornehl et al. [51] attributed the greater dehydrogenation reactivity of UO^+ to participation of the 5f electrons of uranium. Subsequent LAPRD experiments with transuranic AnO^+ indicated a decrease in hydrocarbon activation between UO^+ and NpO^+ [28] which was interpreted in the context of 5f participation in activation and a contraction of the 5f orbitals between uranium and neptunium. In contrast, the present results with silane show no evidence for a decrease in AnO^+ dehydrogenation activity upon proceeding across the series, and instead perhaps a slight increase. One possible explanation for the difference between disilane and alkenes is that the larger and more polarizable silicon atom can interact with the more contracted 5f electrons of the transuranium actinides. It would be expected that further contraction of the 5f electrons beyond Pu would diminish the ability for participation

in Si–H activation—in this context it is unfortunate that insufficient amounts of AmO^+ were ablated to assess the chemistry of this heavier actinide oxide ion. It would also be of interest to examine the chemistry of LnO^+ with disilane because the 4f electrons should be essentially inert.

3.5. Reactions with germane

Comparison of the decomposition enthalpies in Table 3 indicate the substantially lower thermodynamic stability of germane, towards both Ge–H bond cleavage and dehydrogenation, in comparison with methane and silane. Cundari and Gordon [52] have predicted that metal–germylene bonds should be weaker than metal–silylene bonds but many metal germylene complexes have been isolated whereas metal silylenes have proved a more elusive synthetic target [53].

Representative results for metal ion–germane reactions are shown in Figs. 4 and 5, and the results are summarized in Table 2. Because very little attention has been given to the gas phase chemistry of germane, its reactions were studied with Th^+, Ce^+, Tb^+ and Tm^+ as well as with the four An^+ which were reacted with disilane.

From the results in Table 2, it is seen that Th^+, U^+, Np^+ and Tb^+ rather efficiently activate germane to produce the dehydrogenated germylene product, $MGeH_2^+$. In contrast, Pu exhibits minimal reactivity (a very small yield of $PuGeH_2^+$), and both Am^+ and Tm^+ are essentially inert towards germane. Referring to the promotion energies in Table 4, it is evident that germane activation proceeds by insertion of a metal ion into a Ge–H bond to produce a $H–M^+–GeH_3$ intermediate, and that two non-f electrons are required for the two covalent bonds in this intermediate. The mechanism and correlation of reactivities with electron promotion energies is entirely analogous to C–H activation by Ln^+ [8,10] and An^+ [16,28]. Despite that the $H–GeH_3$ bond is $\sim$90 kJ mol^{-1} weaker than the $H–CH_3$ bond (Table 3), the 105 kJ mol^{-1} promotion energy of Pu^+ is clearly manifested as a reduced ability to activate germane, and the metal ion insertion mechanism appears applicable to even the relatively weak Ge–H bond. As with silane, complete dehydrogenation of one germane molecule did not proceed to give the metal monogermanide ion, MGe^+. The bond dissociation energy for neutral ScGe is $\sim$266 kJ mol^{-1} [49], and $\sim$273 kJ mol^{-1} is required to dehydrogenate GeH_4 (Table 3). It would seem feasible that some MGe^+ may form via exothermic dehydrogenation reactions of M^+ with germane. However, kinetic barriers may exclude this reaction channel.

Whereas silane was only partially dehydrogenated, two germane molecules were fully dehydrogenated by the intrinsically reactive ions, Th^+, U^+, Np^+, Ce^+ and Tb^+, to produce the digermanides, MGe_2^+. The mechanism for formation of these species is unclear but the $MGeH_2^+$ are the presumed precursors. Because a species such as $Tb^+{=}GeH_2$ does not possess two free valence electrons at the metal center, it would appear that a simple insertion mechanism is not applicable. One possible scenario is that electrons involved in metal–germanium bonding activate a second germane molecule to generate a short-lived $M^+–\{Ge_2H_4\}$ intermediate which rapidly eliminates two additional H_2 molecules to give MGe_2^+. No MGe^+ species were detected and the rather efficient formation of digermanides can be attributed to stabilization due to Ge–Ge bonding. Although the Ge–Ge and Si–Si bond energies are similar, the complete dehydrogenation of two germane molecules to produce a digermanide is thermodynamically more favorable by $\sim$230 kJ mol^{-1} compared with dehydrogenation of two silane molecules to produce a disilicide (Table 3). Consistent with this, $MSi_2H_{2,4}^+$ were produced while MSi_2^+ were absent. It requires $\sim$270 kJ mol^{-1} to fully dehydrogenate two GeH_4 molecules and produce a Ge_2 dimer so that the $M^+–Ge_2$ bonding energy would have to exceed this value for the observed digermanides to be produced in an exothermic process.

The chemistry of Th^+ with germane was distinctive among all the metal ions studied; Th^+ completely dehydrogenated three and four GeH_4 molecules to produce the polygermanides, $ThGe_3^+$ and $ThGe_4^+$. As has been reported for reactions with hydrocarbons [14,15], Th^+ is even more reactive than U^+.

The ground state of Th^+, [Rn]$6d^2 7s$, is comparable to that of highly reactive third row transition metal ions. For comparison, the ground state of Hf^+ is [Xe]$4f^{14}6d7s^2$, with the [Xe]$4f^{14}6d^2 7s$ configuration 44 kJ mol^{-1} higher in energy.

It requires ~819 kJ mol^{-1} to dehydrogenate three germane molecules and ~1092 kJ mol^{-1} to dehydrogenate four. Gingerich et al. [54] have determined the atomization enthalpies of Ge_3 and Ge_4 as ~590 and ~969 kJ mol^{-1}, respectively. Accordingly, the Th^+–Ge_3 bonding energy must be at least ~229 kJ mol^{-1} and the Th^+–Ge_4 energy at least ~123 kJ mol^{-1} for the observed products to form via exothermic reactions. It is predicted that reaction (11) should be exothermic by ~106 kJ mol^{-1}, due to the evidently especially high special stability of Ge_4.

$$Ge_3 + GeH_4 \rightarrow Ge_4 + 2H_2 \quad (11)$$

The exothermicity of reaction (11) is consistent with the high efficiency of the formation of $ThGe_4^+$ from the reaction of $ThGe_3^+$ with GeH_4; from the values in Table 2 it is evident that the yields of $ThGe_3^+$ and $ThGe_4^+$ were almost the same. The structures of the isolated Ge_3 and Ge_4 clusters have been calculated [55]. For Ge_3, the bent Ge–Ge–Ge (C_{2v}) and cyclo-Ge_3 (D_{3h}) structures are predicted to be nearly energetically degenerate. For Ge_4, the structure is predicted to be that of a cyclo-Ge_4 planar rhombus (D_{2h}).

Peaks are tentatively assigned in Fig. 5 at masses in approximate correspondence to $ThOGe^+$ and $ThOGe_2^+$. Whereas the $ThGe_{1,2,3,4}^+$ products clearly exhibited the isotopic distribution of germanium in the mass spectra, the "$ThOGe_{1,2}^+$" peaks were comparatively very broad and entirely unresolved. This is reminiscent of the nature of the oxide CID peaks. A broad unassigned peak at 75.2 μs, approximately corresponding to $Th[14]^+$ is not shown in Fig. 5; also not shown is the ThO^+ CID peak which appears at the flight time corresponding to "ThH_4^+." It is possible that the low-resolution peaks at higher masses, in analogy with the presumed ThO^+ CID peak, are associated with CID of reaction product ions in the first field-free region of the RTOF-MS. Eq. (5) can be used to predict approximate daughter ion arrival times, t_d, for ions due to the plausible CID processes of Ge-loss from $ThGe_3^+$ and $ThGe_2^+$, and GeH_2-loss from $ThGeH_2^+$. These predicted t_d are within roughly 0.4 to 0.7 μs of the approximate measured arrival times for the low-resolution ion peaks. A deviation from t_d derived from the empirical Eq. (5) for O-loss might be expected because of the greater m_d/m_p associated with Ge-loss.

Also, unresolved peaks in approximate correspondence to "$UOGe^+$" and $U[14]^+$ appeared upon ablation of U^+ into GeH_4—these peaks may have resulted from CID of UGe_2^+ and $UGeH_2^+$, respectively. It should be noted that not all CID peaks which might have been anticipated based on the product mass spectra were definitively identified. Because of the possibility of CID and the anomalous character of the peaks, $MOGe_n^+$ are not reported as products in Table 2. However, it should be emphasized that the possibility of some reactions of ThO^+, and perhaps also UO^+, with germane cannot be confidently excluded based on the present results.

4. Summary

The present study of reactions of selected actinide (and lanthanide) ions with silanes and germane extends our studies of the gas-phase metal ion chemistry in this challenging region of the periodic table. The results with methane and ethane revealed essentially inert behavior for all of the studied ions except Th^+, consistent with the occurrence of only exothermic reactions of ground state metal ions under the experimental conditions employed in the present study. The appearance of what were initially assigned as product ion peaks corresponding to the tetrahydrides, AnH_4^+, was discordant. A series of experiments has led to the conclusion that these aberrant features of the mass spectra were a result of CID of ablated metal oxide ions, MO^+, in the first field-free region of the RTOF-MS. This analysis leads to the nullification of a previous report of the production of actinide tetrahydride ions as a result of the reaction of bare actinide ions with ethylene oxide.

The primary reactions with the silanes were dehydrogenation. In the case of SiH_4, dehydrogenation resulted in the silylenes, $MSiH_2^+$, for the three studied actinide ions, U^+, Np^+ and Pu^+. Dimerization to produce $MSi_2H_{2,4}^+$ also proceeded for M = U and Np. The low reaction efficiency for Pu^+ indicates activation by an insertion mechanism which requires two non-5f electrons at the metal center. With the Si_2H_6 reaction substrate, U^+ and Np^+ induced single- and double-dehydrogenation while Pu^+ and Am^+ were essentially inert, consistent with an insertion-type activation mechanism, as was found for SiH_4. The three MO^+, M = U, Np and Pu, each induced dehydrogenation of disilane with comparable efficiencies, indicating a non-insertion mechanism which involves a multi-centered activated intermediate. Germane was efficiently activated by Th^+, U^+, Np^+, Ce^+ and Tb^+ to produce the germylenes, $MGeH_2^+$. In contrast, Pu^+ was marginally reactive with GeH_4 and both Am^+ and Tm^+ were essentially inert. Again, an insertion mechanism requiring two non-5f electrons is indicated for germane activation. The five reactive M^+ also fully dehydrogenated two GeH_4 molecules to generate the metal digermanides, MGe_2^+ (M = Th, U, Np, Ce and Tb). The typical high reactivity of Th^+, which behaves similarly to a 5d-transition metal ion, was manifested in the formation of $ThGe_3^+$ and $ThGe_4^+$ upon reaction with germane. The results for reactions of MO^+ with germane are considered inconclusive.

As expected, silanes and germane are much more susceptible to activation and dehydrogenation compared with their hydrocarbon homologs (which are nearly inert under comparable conditions). Despite the more fragile character of the Si–H and Ge–H bonds, the comparative metal ion reactivities demonstrate that activation by actinide (and lanthanide) ions proceeds by an insertion mechanism which requires two non-f valence electrons at the metal center. This is analogous to hydrocarbon activation by the f-block metal ions and indicates that the 5f electrons remain chemically inert, even with the larger and more polarizable silanes and germanes. Several new species were produced, including actinide silylenes, germylenes and germanides.

Acknowledgements

Research sponsored by the Division of Chemical Sciences, Geosciences and Biosciences, Office of Basic Energy Sciences, U.S. Department of Energy, under contract DE-AC05-00OR22725 with Oak Ridge National Laboratory, managed and operated by UT-Battelle, LLC.

References

[1] K. Eller, H. Schwarz, Chem. Rev. 91 (1991) 1121.
[2] B.S. Freiser (Ed.), Organometallic Ion Chemistry, Kluwer academic Publishers, Dordrecht, 1996.
[3] Y. Huang, M.B. Wise, D.B. Jacobson, B.S. Freiser, Organometallics 6 (1987) 346.
[4] J.B. Schilling, J.L. Beauchamp, J. Am. Chem. Soc. 110 (1988) 15.
[5] L.S. Sunderlin, P.B. Armentrout, J. Am. Chem. Soc. 111 (1989) 3845.
[6] C. Heinemann, D. Schröder, H. Schwarz, Chem. Ber. 127 (1994) 1807.
[7] W.W. Yin, A.G. Marshall, J.M. Marçalo, A. Pires de Matos, J. Am. Chem. Soc. 116 (1994) 8666.
[8] H.H. Cornehl, C. Heinemann, D. Schröder, H. Schwarz, Organometallics 14 (1995) 992.
[9] J. Marçalo, A. Pires de Matos, W.J. Evans, Organometallics 15 (1996) 345.
[10] J.K. Gibson, J. Phys. Chem. 39 (1996) 15688.
[11] J. Marçalo, A. Pires de Matos, W.J. Evans, Organometallics 16 (1997) 3845.
[12] P.B. Armentrout, R.V. Hodges, J.L. Beauchamp, J. Chem. Phys. 66 (1977) 4683.
[13] C. Heinemann, H.H. Cornehl, H. Schwarz, J. Organomet. Chem. 501 (1995) 201.
[14] J. Marçalo, J.P. Leal, A. Pires de Matos, Int. J. Mass Spectrom. Ion Processes 157/158 (1996) 265.
[15] J. Marçalo, J.P. Leal, A. Pires de Matos, Organometallics 16 (1997) 4581.
[16] J.K. Gibson, Int. J. Mass Spectrom. 214 (2002) 1.
[17] H. Kang, D.B. Jacobson, S.K. Shin, J.L. Beauchamp, M.T. Bowers, J. Am. Chem. Soc. 108 (1986) 5668.
[18] K.K. Irikura, J.L. Beauchamp, J. Am. Chem. Soc. 111 (1989) 75.
[19] M. Decouzon, J.-F. Gal, S. Géribaldi, M. Rouillard, J.-M. Sturla, Rapid Commun. Mass Spectrom. 3 (1989) 298.
[20] M. Azzaro, S. Breton, M. Decouzon, S. Géribaldi, Rapid Commun. Mass Spectrom. 6 (1992) 306.
[21] D.B. Jacobson, R. Bakhtiar, J. Am. Chem. Soc. 115 (1993) 10830.
[22] B.L. Kickel, P.B. Armentrout, J. Am. Chem. Soc. 116 (1994) 10742.
[23] B.L. Kickel, P.B. Armentrout, J. Am. Chem. Soc. 117 (1995) 764.

[24] B.L. Kickel, P.B. Armentrout, J. Am. Chem. Soc. 117 (1995) 4057.
[25] B.L. Kickel, P.B. Armentrout, J. Phys. Chem. 99 (1995) 2024.
[26] A. Ferhati, T.B. McMahon, G. Ohanessian, J. Am. Chem. Soc. 118 (1996) 5997.
[27] M. Bronstrup, D. Schröder, H. Schwarz, Chem.-A Eur. J. 5 (1999) 1176.
[28] J.K. Gibson, J. Am. Chem. Soc. 120 (1998) 2633.
[29] Y.A. Ranasinghe, T.J. MacMahon, B.S. Freiser, J. Phys. Chem. 95 (1991) 7721.
[30] (a) S.G. Lias, J.E. Bartmess, J.F. Liebman, J.L. Holmes, R.D. Levin, W.G. Mallard, Gas-Phase Ion and Neutral Thermochemistry, American Chemical Society, Washington, DC, 1988;
(b) W.G. Mallard (Ed.), NIST Chemistry WebBook, NIST Standard Reference Database Number 69, U.S. Department of Commerce, Washington, DC, 2001 (http://webbook.nist.gov/chemistry/).
[31] R.J. Cotter, Time-of-Flight Mass Spectrometry, American Chemical Society, Washington, DC, 1997, pp. 53, 170.
[32] I.S. Gilmore, M.P. Seah, Appl. Surface Sci. 144/145 (1999) 26.
[33] P.B. Armentrout, J.L. Beauchamp, Chem. Phys. 50 (1980) 21.
[34] M.R. Sievers, Y. Chen, P.B. Armentrout, J. Chem. Phys. 105 (1996) 6322.
[35] K.R. Jennings, Int. J. Mass Spectrom. Ion Phys. 1 (1968) 227.
[36] W.F. Haddon, F.W. McLafferty, J. Am. Chem. Soc. 90 (1968) 4745.
[37] F.W. McLafferty, H.D.R. Schuddemage, J. Am. Chem. Soc. 91 (1969) 1866.
[38] I.V. Chernushevich, A.N. Verentchikov, W. Ens, K.G. Standing, J. Am. Soc. Mass Spectrom. 7 (1996) 342.
[39] K.F. Medzihradszky, J.M. Campbell, M.A. Baldwin, A.M. Falick, P. Juhasz, M.L. Vestal, A.L. Burlingame, Anal. Chem. 72 (2000) 552.
[40] F.W. McLafferty, P.F. Bente III, R. Kornfeld, S.-C. Tsai, I. Howe, J. Am. Chem. Soc. 95 (1973) 2120.
[41] B. Spengler, D. Kirsch, R. Kaufmann, J. Phys. Chem. 96 (1992) 9678.
[42] J.A. Fayeton, M. Barat, J.C. Brenot, H. Dunet, Y.J. Picard, U. Saalmann, R. Schmidt, Phys. Rev. A 57 (1998) 1058.
[43] J.K. Gibson, J. Mass Spectrom. 36 (2001) 284.
[44] B. Ruscic, M. Schwarz, J. Berkowitz, J. Chem. Phys. 92 (1990) 1865.
[45] B. Ruscic, J. Berkowitz, J. Chem. Phys. 95 (1991) 2416.
[46] J. Blaise, J.-F. Wyart, International Tables of Selected Constants, 20, Energy Levels and Atomic Spectra of Actinides, Tables Internationales de Constantes, Paris, 1992.
[47] W.C. Martin, R. Zalubas, L. Hagan, Atomic Energy Levels—The Rare Earth Elements, National Bureau of Standards (NIST), Washington, DC, 1978.
[48] P.B. Armentrout, in: D.H. Russell (Ed.), Gas Phase Inorganic Chemistry, Plenum Press, New York, 1989, pp. 1.
[49] J.E. Kingcade Jr., K.E. Gingerich, J. Chem. Soc., Faraday Trans. 2 85 (1989) 195.
[50] H.H. Cornehl, R. Wesendrup, J.N. Harvey, H. Schwarz, J. Chem. Soc., Perkin Trans. 2 (1997) 2283.
[51] H.H. Cornehl, R. Wesendrup, M. Diefenbach, H. Schwarz, Chem. Eur. J. 3 (1997) 1083.
[52] T.R. Cundari, M.S. Gordon, J. Phys. Chem. 96 (1992) 631.
[53] W. Petz, Chem. Rev. 86 (1986) 1019.
[54] K.A. Gingerich, M.S. Baba, R.W. Schmude Jr., J.E. Kingcade Jr., Chem. Phys. 262 (2000) 65.
[55] E.F. Archibong, A. St-Amant, J. Chem. Phys. 109 (1998) 962.